Journal of Materials Chemistry A

PAPER

View Article Online
View Journal | View Issue



Cite this: J. Mater. Chem. A, 2016, 4, 7875

# Improved photoelectrochemical performance of electrodeposited metal-doped $BiVO_4$ on Pt-nanoparticle modified FTO surfaces†

Ramona Gutkowski,[a] Daniel Peeters[b] and Wolfgang Schuhmann*[a]

Received 13th February 2016
Accepted 25th April 2016

DOI: 10.1039/c6ta01340f

www.rsc.org/MaterialsA

The recombination of photogenerated electron–hole pairs is one of the main limiting factors of photoelectrocatalysts absorbing in the visible part of the solar spectrum. Especially for $BiVO_4$ the slow electron transport to the back contact facilitates charge recombination. Hence, thin layers have to be used to obtain higher photocurrents which are concomitantly only allow low absorption of the incident light. To address this limitation we have modified FTO substrates with Pt-nanoparticles before electrodepositing $BiVO_4$. The Pt-nanoparticles decrease the overpotential for the electrodeposition of $BiVO_4$, but more importantly they provide the basis for decreased charge recombination. Electrodeposited Mo-doped $BiVO_4$ on Pt-nanoparticle modified FTO exhibits a substantially decreased recombination of photogenerated charge carriers during frontside illumination. Simultaneous co-doping of $BiVO_4$ with two different metals leads to a substantial enhancement of the incident-photon-to-current efficiency (IPCE) during light driven oxygen evolution reaction. Highest IPCE (>30% at 1.2 V *vs.* RHE) values were obtained for Mo/Zn- and Mo/B-doped $BiVO_4$.

## Introduction

Suitable materials for solar water splitting have to fulfil a number of prerequisites. The oxygen evolution reaction (OER) is the limiting half-cell reaction due to high overpotentials necessary for the four electron-transfer reaction. N-type semiconductors with low band gaps (<3.0 eV) are required for absorbing in the visible part of the solar spectrum. Thus, due to its band gap of about 2.4 eV [1–3] and its band position suitable for oxygen evolution[4] $BiVO_4$ is regarded as a promising material for solar water splitting.[5–12] $BiVO_4$ can be deposited onto FTO substrates *e.g.* by a metal–organic-decomposition method followed by spin-coating[13–17] or drop-casting.[18] Seabold *et al.* developed a simple procedure for the electrodeposition of $BiVO_4$ from a bismuth nitrate and vanadyl sulfate precursor solution,[19] while Jiang *et al.* used an inkjet printer[3] for $BiVO_4$ deposition. Independent of the preparation method, due to the poor electron-transfer kinetics leading to high recombination rates of photo-generated electron–hole pairs $BiVO_4$ films are not suitable for solar-energy conversion using frontside illumination. $BiVO_4$ provides higher photocurrents or incident-photon-to-current efficiencies (IPCE) upon backside illumination.[20,21] A variety of strategies to improve the photoelectrochemical performance of $BiVO_4$ were suggested such as among others doping with different metals. For example doping with molybdenum,[22–29] tungsten[30–34] or simultaneously with two different metals[18] leads to an increase in electron density of the doped $BiVO_4$ resulting in higher IPCE values. To prevent the accumulation of photogenerated holes at the semiconductor/electrolyte interface due to slow OER kinetics, co-catalysts were deposited on $BiVO_4$.[16,31,35–42] Moreover, using reduced graphene oxide, Kudo *et al.* were able to promote electron-transfer resulting in higher IPCE values.[43]

Next to the above presented strategies for enhancing the photoelectrochemical performance of suitable photoabsorber materials, the insertion of interfacial layers, nanoparticles, nanotubes and nanowires, *e.g.* $WO_3$ or CNTs offers a strategy to increase the charge carrier life time upon illumination with solar energy.[15,44–51] We purpose as an alternative strategy the modification of the FTO substrate with Pt-nanoparticles prior to the electrochemically induced $BiVO_4$ deposition. The presence of these nanoparticles slightly decreases the overpotential of anodic $BiVO_4$ formation improving the low conductivity of the FTO substrate and provide nuclei centres for film growing. However, more importantly the presence of the Pt-nanoparticles within Mo-doped $BiVO_4$ films gave rise to higher IPCE values due to decreased recombination rate of photogenerated electron–hole pairs. Doping of $BiVO_4$ with Mo or W was found to

[a]Analytical Chemistry – Center for Electrochemical Science (CES), Ruhr-Universität Bochum, Universitätsstr. 150, D-44780 Bochum, Germany. E-mail: wolfgang.schuhmann@rub.de

[b]Inorganic Chemistry II, Ruhr-Universität Bochum, Universitätsstr. 150, D-44780 Bochum, Germany

† Electronic supplementary information (ESI) available: Additional information contain further characterization (Raman and EDX measurements), band gap determination from wavelength dependent photocurrent spectroscopy and SEM images of the different doped $BiVO_4$ films. Optimization of the Pt-NP deposition on FTO substrates is shown. See DOI: 10.1039/c6ta01340f

improve additionally the photocatalytic efficiency. By doping of $BiVO_4$ simultaneously with two metals by means of electrodeposition on Pt-nanoparticle modified FTO substrates highest IPCE values were obtained for Mo/Zn and Mo/B doped $BiVO_4$.

## Experimental part

Fluorine-doped tin oxide (FTO) substrates (Pilkington, TEC 8A, 2.3 mm) were first cleaned with acetone under ultra-sonication for 5 min followed by a treatment in 0.1 M NaOH (99%) for 15 min at 75 °C. After rinsing with water the FTO were dried in an Ar stream. All chemicals were from Sigma Aldrich if not mentioned otherwise. All electrochemical measurements were carried out in a three-electrode setup with an Ag/AgCl/3 M KCl (210 mV *vs.* NHE) reference electrode and a Pt wire counter electrode. Pt-nanoparticles[52,53] were electrochemically deposited from a 0.4 mM $H_2PtCl_6$ (ACS reagent, ≥37.50% Pt basis) solution by applying potential pulses using a graphite rod counter electrode. A no-effect potential of 0 V was applied for 1 s, while deposition was performed for 0.2 s at −1 V. The potential pulse sequence was repeated 50 times. For the fabrication of the $BiVO_4$ films, the electrodeposition procedure of Seabold *et al.* was adapted.[19] In short, 35 mM $VOSO_4 \cdot H_2O$ (≥97%) were diluted in 0.54 M $HNO_3$ and 10 mM $Bi(NO_3)_3 \cdot 5H_2O$ (≥98%) were added. For increasing the pH value up to 5, 2 M sodium acetate tetrahydrate (VWR, 100%) was used for stabilizing the Bi(III)-ions. The pH value was adjusted to 4.7 with conc. $HNO_3$. Electrodeposition was performed at 1.9 V *vs.* Ag/AgCl/3 M KCl at 70 °C using a circulation thermostat and a Pt-mesh as counter electrode. It should be mentioned that the counter electrode was separated by means of a membrane from the deposition solution to prevent precipitation of Bi(0) at the Pt counter electrode. 2 M sodium acetate solution (pH 4.7) was used as electrolyte. The deposition was taking place for 400 s and 600 s on bare FTO and FTO modified with Pt-nanoparticles. The FTO substrates were contacted with an aluminium foil which was insulated during deposition with parafilm. For doping, 5 mM of the additional precursor salt was added to the described Bi–V-solution. For doping with two different metals 5 mM of each precursor salt was found to be best for depositing homogenous layers and providing high photocurrents. $Zn(NO_3)_2 \cdot 6H_2O$ (≥99%), $Na_2WO_4 \cdot 2H_2O$ (≥99%), $Pb(NO_3)_3$ (Riedel-de-häen, 99%), $NaMoO_4$ (≥99%), $MnSO_4$ (≥99%), $Fe(NO_3)_3 \cdot 9H_2O$ (Acros, ≥99%), $H_3BO_3$ (J.T. Baker, ≥99.9%) were used for co-doping and were added directly before the electro-chemically induced deposition. After electrodeposition a brownish film was obtained, which turned into yellow after annealing in air at 500 °C for 1 h with a heating rate of 2 °C $min^{-1}$. To remove vanadium pentoxide the samples were treated with 1 M KOH for 20 min.

Photocurrent spectroscopy was performed using a microprocessor controlled monochromatic system (Institut Fotonowy) with integrated shutter. A short pass filter (<400 nm) and a long pass filter (>400 nm) were utilized to remove completely the undesired part of the spectrum. A 150 W Xe-Lamp (Ushio) was used as light source. All measurements were done in pyrex glass cell. If the samples were irradiated from the front, the light passes through a quartz window. The irradiated area was 0.785 $cm^2$. The power of the incident light was determined with a power meter (Thorlabs) and a thermopile detector and was corrected by the power loss of the quartz window.

An Autolab PGSTAT12 (Metrohm) potentiostat was used to apply an external bias potential. Light induced water splitting was performed in 0.1 M $Na_2SO_4$ (p.a.) as electrolyte at a pH value of 6. The applied potential ($E_{app}$) was re-calculated *versus* the reversible hydrogen electrode (RHE) by $E(RHE) = 210\ (mV) + E_{app} + 59 \times pH$. The obtained photocurrents $i_{ph}$ were derived by subtracting the dark current from the current measured under illumination (ESI, Fig. S1†) and the IPCE was calculated taking the photon flux ($\Phi(\lambda)$) for each wavelength into account (eqn (1)). $e$ represents the elementary charge.

$$IPCE = i_{ph}(\lambda)/e\Phi(\lambda) \quad (1)$$

## Results and discussion

### Single doping of $BiVO_4$

Before studying the influence of the back contact-modification by means of Pt-nanoparticles on the photoelectrocatalytic performance of $BiVO_4$ or metal-doped $BiVO_4$ the electrochemically induced deposition of $BiVO_4$ films had to be optimized to achieve highest possible IPCE values (Fig. 1).

Seabold *et al.* achieved IPCE values of <5% at 1.2 V *vs.* RHE (pH 7) of undoped $BiVO_4$ films,[19] while Ding *et al.* reached up to 10% at 0.5 V *vs.* SCE (pH 9) using longer deposition times.[20] These difference are attributed to the layer thickness, which is proportional to the IPCE, where very thin layers (<100 nm) results in highest IPCE values close to 40% during frontside illumination.[21] Fig. 1 summarizes the obtained IPCE values at

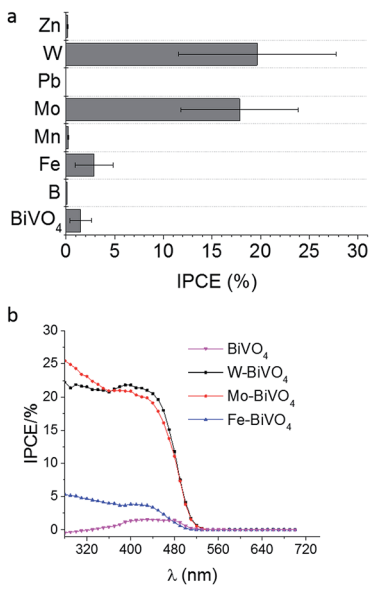


Fig. 1 IPCE values at 450 nm and 1.2 V *vs.* RHE for differently doped $BiVO_4$ films deposited on Pt-nanoparticle modified FTO (a) and IPCE spectra using frontside illumination (b).

450 nm and 1.2 V *vs.* RHE bias potential for differently doped $BiVO_4$ films compared with undoped $BiVO_4$. Highest IPCE values of up to 18–20% were obtained for W- and Mo-doped $BiVO_4$ films on Pt-nanoparticle modified FTO substrates. Doping with Fe is slightly increasing the photoelectrocatalytic efficiency, while doping with B, Mn, Zn and Pb had a negative effect leading to lower IPCE values as compared with undoped $BiVO_4$ films. These results coincide with the screening of different metal-doped $BiVO_4$ shown by Parmar *et al.*[17] using the metal–organic-decomposition method and spin-coating. The IPCE spectra for the Fe, Mo, and W-doped $BiVO_4$ films indicate a small increase of the band gap for Fe-doped $BiVO_4$ (Fig. 1b). Concerning the band gap, direct[1,18] or indirect[3,48] transition is assumed for monoclinic $BiVO_4$. The derived IPCE values demonstrate photocatalytic activity of up to 530 nm suggesting a band gap of 2.3 eV. Additionally, UV-vis absorption spectra support this finding (ESI, Fig. S3†). An indirect band gap of 2.3 eV was calculated from Tauc-plots, while a direct band gap of 2.4 eV was derived for Mo-doped $BiVO_4$ (ESI, Fig. S1 and S2†). Recently published results from Cooper *et al.* suggest also an indirect band-to-band transition.[54]

### Concept of Pt-nanoparticle modification

Regarding the electrochemically induced deposition of semiconductor materials, the low conductivity of the used FTO substrates is leading to a high overpotential for Bi–V–O formation. Decorating the surface of the FTO with Pt-nanoparticles (50 nm diameter), small nuclei for film growth are created, thus reducing the overpotential for film formation.

With increasing deposition time the Bi–V–O film is formed initially at the Pt and then in there vicinity, leading finally to a fully covered surface with a large number of small metal cores (Fig. 2b). In the simplest case, recombination of the photogenerated electron–hole pairs and in particular the absorption of the incident light depend on the layer thickness of the semiconductor material. For thick layers ($d_1$) light absorption increases, but the recombination rate increases due to a longer diffusion length of electrons. This has a tremendous impact on the photoelectrochemical performance. In case 1 in Fig. 2a, lower photocurrents are expected for a thick layer ($d_1$). A decrease of the recombination rate ($r_2$) is possible by reducing the layer thickness ($d_2$, case 2). However, by this the absorption of the incident light is concomitantly decreased limiting the PEC performance. The introduction of small Pt-nanoparticles (Fig. 2b) decrease the recombination rate at the interfacial layer between the photoabsorber and the FTO for the same layer thickness ($d_1$) with good absorption of the incident light by electron capturing. Moreover, the advantage of the deposition of the Pt-nanoparticles *e.g.* over a backside metal film is seen in the ability of utilizing transparent films for tandem cell applications with an improved homogeneity of the deposited semiconductor layer on the metal nuclei. For creating uniform Pt-nanoparticles with a small diameter on the FTO surfaces sequences of potential pulses were used as reported previously.[52,53] The density of the nanoparticle distribution was controlled by the number of repetitions of these pulses.

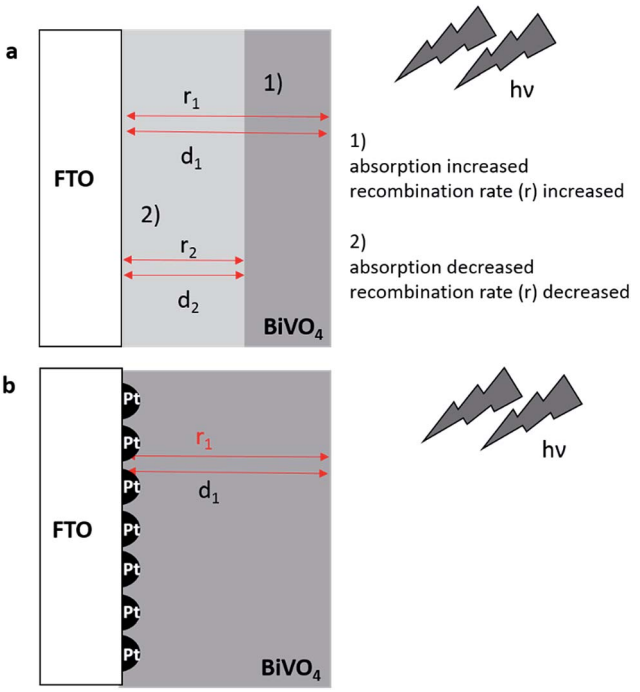


Fig. 2 Mo-doped $BiVO_4$ films deposited on bare FTO (a) for two different cases for thick (1) or thin (2) layers. Effect of Pt-nanoparticles on the recombination rate *r* and the absorption of the incident light depending on the layer thickness *d* (b).

Optimal conditions for uniformly sized and high density distributed Pt-nanoparticles were obtained by repeating the deposition pulses 50 times (ESI, Fig. S3†). Higher repetition numbers lead to Pt nanoparticles with increased diameter and lower density. Finally agglomeration was noticed at a 110 pulse sequence. The correlation of pulse sequences and loading of the Pt-nanoparticle is demonstrated in Fig. S4.† It is expected that the deposition of the Pt nanoparticles on FTO exhibit a substantial impact on the hydrogen evolution reaction (HER).[55] An increase of the HER current was observed until a number of 110 Pt nanoparticle deposition pulse sequences. No further changes of the cathodic HER current were noticed between 110 until 350 deposition pulse sequences. In comparison to unmodified FTO, loading with Pt-nanoparticles increased the HER activity significantly with lower deposition pulse sequence number.

The influence of Pt-nanoparticles on the photocatalytic performance was studied using Mo-doped $BiVO_4$ films because these films showed higher reproducibility as compared to W-doped $BiVO_4$ (see Fig. 1). First, the effect of the deposited Pt-nanoparticle on the layer thickness was evaluated. Although electrode-position leads to comparatively rough surfaces, SEM cross-section allowed to estimate the layer thickness (Fig. 3).

Mo-doped $BiVO_4$ films were prepared in absence and presence of Pt-cores on the FTO surface and a similar layer thickness of around 600 ± 50 nm was obtained in both cases. Reducing the deposition time to 400 s, the layer thickness decreased around 450 ± 50 nm (ESI, Fig. S5†). These results indicate on the one side, that the layer thickness is increasing with the

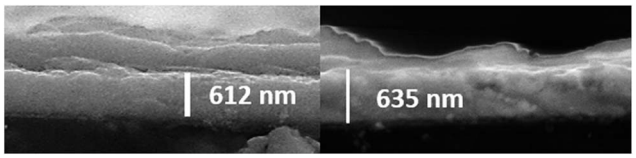


Fig. 3 SEM cross-sections of Mo-doped $BiVO_4$ films deposited in absence of Pt-nanoparticles (left) and in presence of Pt-nanoparticles on FTO (right).

deposition time. On the other side, for small Pt-nanoparticles (50 nm) no influence on the film electrodeposition was observed resulting in comparable film thicknesses for layers deposited in presence and in absence of Pt-nanoparticles. Comparable layer thicknesses in accordance with the model in Fig. 2 is necessary to evaluate the effect of the Pt-nanoparticles on the recombination process during PEC measurements. Frontside illumination was used to demonstrate the impact of the Pt-cores on the photocatalytic properties of the Mo-doped $BiVO_4$ films. It was anticipated that in presence of Pt-nanoparticles the electron transfer is facilitated leading to a substantially decreased charge-carrier recombination. Mo-doped $BiVO_4$ films were deposited in absence and in presence of Pt-nanoparticles on FTO surfaces for 400 s and 600 s and the IPCE values were determined (Fig. 4a). At a wavelength of 450 nm an increase in the IPCE was observed when the FTO was modified with Pt-nanoparticles. This suggests a higher PEC performance due to an improved absorption of the incident light at thicker films (600 nm ± 50 nm) and an enhanced PEC performance in presence of Pt-nanoparticles.

In a chronoamperometric experiment at a defined bias potential of 0.5 V *vs.* RHE the shutter of the lamp was opened and closed for predefined times. During the dark current measurement the wavelength was changed in a range from 250 nm to 550 nm (Fig. 4b). This current–time response hence does not only provide information about the wavelength-dependent photocurrent which is the basis for the determination of wave-length-dependent IPCE values, but it provides information about the recombination rate of the photogenerated electron–hole pairs. The initial current peak ($i_{init}$) measured directly when the lamp shutter was opened represents the separation of electrons and holes in the depletion region. The decay of the current results from holes, which recombine with electrons from the CB or accumulate at the surface instead of reacting with electrons from the electrolyte.[56–59] The time dependent decay of the current under continuous illumination until a steady-state current ($i_{ss}$) is established, based on the recombination of holes in the VB with electrons from the CB, produced when the light reached for the first time the surface. This current is based on holes which did not recombine and contribute to the faradaic process.[56,60] The steady state current is influenced by the recombination process at the interfacial layer and is decreased if recombination centres at the substrate are present. Moreover, this current depends on the kinetics of the reaction at the semi-conductor/electrolyte interface. Slow kinetics increases surface recombination and decreases the photocurrent. The lower the difference between

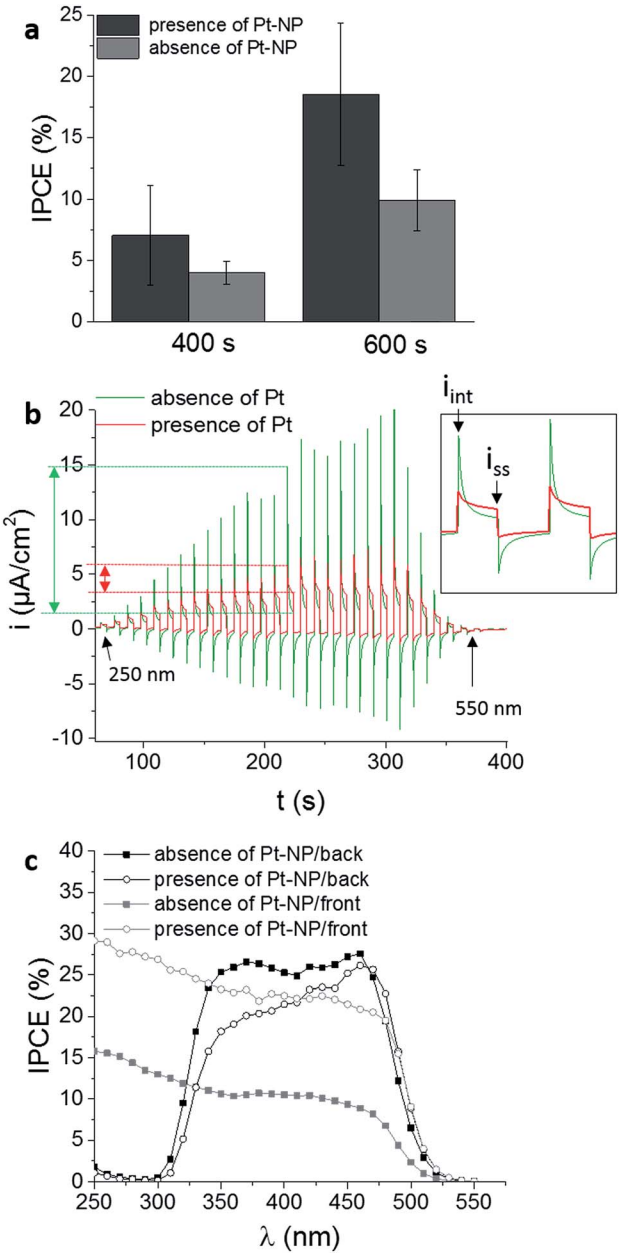


Fig. 4 (a) IPCE values at 450 nm and a bias potential of 1.2 V *vs.* RHE in 0.1 M $Na_2SO_4$ for Mo-doped $BiVO_4$ films deposited for 400 s or 600 s on bare or Pt-nanoparticles modified FTO surfaces. (b) Current–time response at a bias potential of 0.5 V *vs.* RHE for a Mo-doped $BiVO_4$ films obtained with a deposition time of 600 s. During opening and closing the lamp shutter the wavelength of the incident light was increased from 250 to 550 nm. Insert: representation of the initial current ($i_{init}$) and the steady-state current ($i_{ss}$). (c) Wavelength-dependent IPCE values with and without Pt-cores inside the Mo-doped $BiVO_4$ film for illumination from the front and back.

$i_{init}$ and $i_{ss}$ the lower is the overall recombination rate. As a matter of fact this difference is influenced by the applied bias potential *i.e.* with increasing bias potential $i_{init}$ decreases and $i_{ss}$ increases (ESI, Fig. S6†).[57] In order to analyse the effect of Pt-nanoparticles on the charge recombination rate a bias potential close to the open circuit potential (0.5 V *vs.* RHE) was

 

applied (Fig. 4b). Consequently, the charge carrier life time is enhanced, if the ratio of the steady state current and initial current under illumination is close to one. Under comparable conditions, the ratio under illumination at 350 nm is relatively low (0.12) for Mo-$BiVO_4$ deposited in absence of Pt-nanoparticles on FTO. The ratio increased up to four times (0.46) by in the insertion of Pt-nanoparticles between the Mo-$BiVO_4$ layer and the FTO surface, indicating a decreased recombination of photogenerated charge carriers thus leading concomitantly to the observed higher photocurrents.

Moreover, the same samples were investigated using backside illumination through the FTO substrate (Fig. 4c). For Mo-doped $BiVO_4$ films an improvement of the electron transport is expected due to the increased electron density caused by doping with Mo. Thus, higher photocurrents are anticipated during frontside illumination as compared with backside illumination.[21,28,56] For electrodeposited Mo-doped $BiVO_4$ on a bare FTO substrate with a thickness of the film of around 600 nm, higher IPCE values are observed for backside illumination despite the insertion of Mo into the lattice.

The IPCE values increased from around 10% to nearly 25% in the wavelength range between 350 nm and 450 nm. In this case the electron transfer to the back contact seems to be limiting. Seabold *et al.* observed similar effects. Thick films of several hundred nm provide higher photocurrents under backside illumination attributed to the small diffusion length of electrons of around 300 nm.[22] Thin layers (<300 nm) usually exhibit higher photocurrents under frontside illumination. For Mo-doped $BiVO_4$ films deposited on FTO modified with Pt-nanoparticles with a thickness of around 600 nm the differences between frontside and backside illumination decreased (see for details Fig. S7, ESI†). Accordingly, introduction of Pt-nanoparticles at the back contact improves electron transfer and suppresses recombination of photogenerated electron–hole pairs expecting same kinetic rates for the OER in both cases. This supports additionally the hypothesis of improved electron transfer *via* the Pt-nanoparticles.

Assuming direct contact between FTO and Mo-doped $BiVO_4$ (Fig. 5a) the electrons have to diffuse through the semiconductor to the back contact, which is supposed to be limiting during frontside illumination due to the high recombination rates for photogenerated electron–hole pairs. Backside illumination reduces the diffusion length for electrons to the back contact, hence decreasing the recombination rate and terminally leading to higher photocurrents. A possible explanation of this effect is the passivation of the recombination centres of the FTO substrate, reducing the recombination of charge carriers at the interfacial layer.[48] Moreover, by modifying FTO with Pt-nanoparticles a Schottky barrier between platinum and the Mo-doped $BiVO_4$ film is generated due to the higher work function of platinum.[61] Under illumination and by applying an external bias potential the photogenerated electrons can pass the energy barrier between the Pt/semiconductor contact (Fig. 5b) and are no longer available for recombination. This could explain the observed higher IPCE values as compared to Mo-doped $BiVO_4$ films deposited in absence of Pt-nanoparticles (Fig. 4). The energy of the electrons seems to be high enough to reach the metal despite the energy barrier, while the electrons are not diffusing back to the semiconductor due to the energy barrier and the induced electric field caused by applying the external bias.

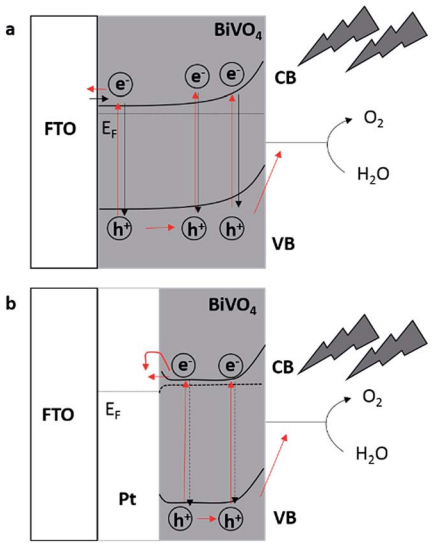


Fig. 5 Schematic representation of recombination processes and diffusion path-ways of photogenerated electron–hole pairs in Mo-doped $BiVO_4$ films deposited (a) on FTO and (b) on FTO modified with Pt-nanoparticles with the same layer thickness.

## Co-doping of $BiVO_4$

The concept of modifying FTO substrates with Pt-nanoparticles was additionally used to further improve the photoelectrochemical performance of doped $BiVO_4$ films by co-doping with two different metals during film electrodeposition. In contradiction to the results obtained by Park *et al.*,[18] who obtained a moderate enhancement to maximum IPCE values of 12% with drop-casted W/Mo-doped $BiVO_4$ films, co-doping was performed by adding a second element (Pb, Zn, B) to Mo, because the electro-deposition of Mo-$BiVO_4$ on top of Pt-nanoparticles already yielded IPCE values up to 25%. First, the morphology and structure of the supposed metal-doped electrodeposited $BiVO_4$ films were analysed. A possible difference in the photocatalytic efficiency is expected due to the changes of the morphology of the deposited film by adding an additional metal salt to the deposition bath (ESI, Fig. S4†). Undoped and W-doped $BiVO_4$ form rough particles, while the overall size of these particles decreased by doping with W. Doping with Mo and an additional element like Zn and B, smaller, rounder and smoother particles are observed compared to undoped $BiVO_4$ and Mo-$BiVO_4$. Electrochemical deposition of $BiVO_4$ in presence of a B or Zn precursor, led to flat and agglomerated particles forming a dense layer. This change of the particle morphology suggests the formation of Zn–Bi–V–O films during the electrodeposition and annealing procedure. Similar to Mo/Zn doping, the W-$BiVO_4$ particles changed to a rounder shape in presence of a Zn precursor during the deposition. The effect of the doping of $BiVO_4$ films were further characterized by means of XRD and

EDX analysis (ESI; Fig. S9 and S10†). XRD patterns do not show any additional reflections from impurities such as $MoO_x$ or ZnO. However, the formation of the monoclinic scheelite structure is obvious, while a shift of the characteristic peak at 28.9°, which is attributed to the incorporation of $Mo^{6+}$ instead of $V^{5+}$ into the monoclinic $BiVO_4$ structure.[18] Merging of the peaks at 34.5° and 35.2° as well as the peaks at 46.8° and 47.4° into a single peak suggests the deformation of the scheelite structure.[62] EDX analysis showed small amounts of Zn (<1%). In the case of Mo/Zn doping, small Zn peaks demonstrate the presence of Zn in the material (ESI; Fig. S10†).

Raman spectroscopy (ESI; Fig. S11†) represents a more sensitive method to evaluate the doping of the $BiVO_4$. Similar to XRD patterns, the shift of the symmetric stretching mode of V–O of the Raman band of 833 $cm^{-1}$, indicates an incorporation of an additional metal into the $VO_4^{3-}$ tetrahedron. This stretching frequency belongs to the length of the metal bond and the above-mentioned shift to lower wavenumber suggesting an increase of the bond length. Eqn (2) determines the exponential dependence of the Raman frequency ($\nu$) on the radius ($r$).[63]

$$\nu\ (\mathrm{cm}^{-1}) = 21\ 349 \exp(-1.9176r\ (\text{Å})) \quad (2)$$

For un-doped $BiVO_4$ the metal bond length was calculated to be 1.6916 Å. Doping with Mo increases the bond length to 1.6979 Å and the co-doping with Mo/B or Mo/Zn to 1.701 Å. From material characterization, doping simultaneously with two elements by means of the electrodeposition method was suggested.

The photoelectrochemical performance in dependence of the different dopants combinations for $BiVO_4$ on top of Pt-nanoparticles, exhibits no improvement of the IPCE values upon co-doping with Pb as compared to pure $BiVO_4$. All other materials improved the IPCE values (Fig. 6a and b). For $BiVO_4$ doped with W and an additional element, only co-doping with W/Zn and W/B increased the IPCE values as compared to only W-doped $BiVO_4$. The low reproducibility of the W deposition might be caused by the difficult co-precipitation during the $V^{4+}$-oxidation. These results are in contrast to the results reported by Park *et al.*,[18] who did not observe any improvement for drop-casted co-doped W/Zn-$BiVO_4$ films as compared to W-doped $BiVO_4$ films. Also Berglund *et al.* reported an increase of the IPCE values of up to 30% by doping $BiVO_4$ with W/Mo.[62] The differences during co-doping are probably due to the difference in the ratio of the co-dopants which are caused by the different preparation techniques, influencing the photoelectrochemical performance. We additionally combined Mo with different elements as co-dopants for $BiVO_4$ (Fig. 6b). The effect on the IPCE values coincides with the results for W-doped $BiVO_4$ as shown in Fig. 6a.

The highest IPCE values were reached for Mo/Zn- and Mo/B-co-doped $BiVO_4$ films deposited on top of Pt-nanoparticles for a deposition time of 600 s (Fig. 6d). The difference between the co-doped and the single doped Mo-$BiVO_4$ (Fig. 6c) were significantly higher as compared to W-doped $BiVO_4$ films. The photoelectrochemical performance of Mo-doped $BiVO_4$ could be substantially improved and IPCE values of up to 40% were

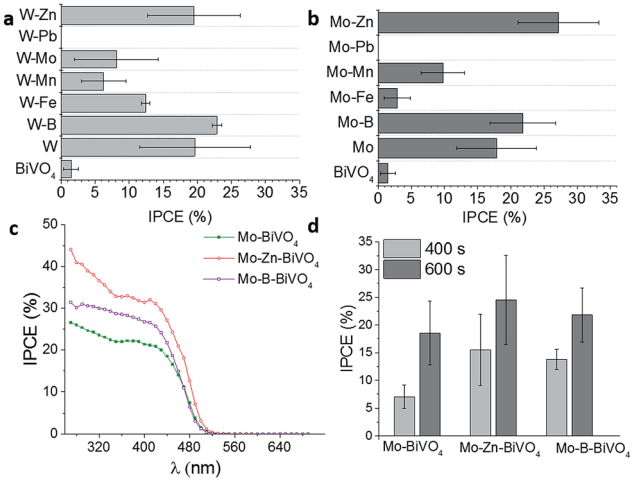


Fig. 6 IPCE values at 450 nm for $BiVO_4$ doped with (a) W and a second element and with (b) Mo and a second element compared to un-doped and single W- or Mo-doped $BiVO_4$ films. Wavelength-dependent IPCE spectra for Mo-doped $BiVO_4$ as well as Mo/Zn- and Mo/B-doped $BiVO_4$ films (c). Influence of the electrodeposition time for different doped $BiVO_4$ films at 450 nm. All measurements were performed in 0.1 M $Na_2SO_4$ at a bias potential of 1.2 V *vs.* RHE (d).

reached under frontside illumination (Fig. 6c). The exact mechanism of the co-doping is not fully understood. As already mentioned, Mo and W are well known donor-type atoms and preferentially substitute V sites. From DFT calculations performed by Yin *et al.*,[64] Zn was suggested to act as an acceptor atom with shallow transition energy for Bi sites compared to V site substitution. Shan *et al.*[65] reported enhanced PEC performance of $BiVO_4$ upon B-doping attributed to the formation of weak chemical bonds between the B-ions and the corners of the $VO_4$-tetrahedron. Additionally, higher photocatalytic activity of B-doped $BiVO_4$ was observed by Wang *et al.*,[66] who supposed synergetic effects of a number of factors created by B-doping, *e.g.* higher specific area or more oxygen vacancies. This might explain the further improvement of the IPCE in the case of Mo/B and Mo/Zn also supported by the different particle shape (see Fig. S4†).

## Conclusion

A different way to improve the absorption of the incident light with increasing the layer thickness resulting in higher IPCE values was demonstrated for Mo-doped $BiVO_4$. The associated decrease of the charge carrier life time limiting the photoelectrochemical performance was circumvented by the introduction of Pt-cores between the Mo-$BiVO_4$ layer and the FTO surface. Two times higher IPCE values were generated in presence of Pt-nanoparticles acting as an electron scavenger preventing the electrons to recombine with the holes in the valence band. The integration of Pt-nanoparticles at the back contact of the Mo-doped $BiVO_4$ film leads to a decrease in the recombination rate of photogenerated electron–hole pairs, which mainly represents next to the kinetic of water oxidation a limiting factor for light induced oxygen evolution at $BiVO_4$

films. Additionally, Pt-nanoparticles favour electrochemically induced deposition of $BiVO_4$ or doped $BiVO_4$ films by improving the conductivity of the FTO substrate. Furthermore, the electrodeposition method can be used to simultaneously dope $BiVO_4$ with different elements by adding an additional precursor compound to the deposition bath. Doping with Mo/Zn and Mo/B leads to a further substantial increase in the IPCE values due to an enhanced electronic conductivity.

## Acknowledgements

The authors are grateful to the DFG in the framework of the SPP1613 (SCHU929/12-1 and 12-2) and the Cluster of Excellence "Resolv" (EXC1069). Bastian Mei is acknowledged for performing the UV-Vis analysis.

## References

1 S. P. Berglund, D. W. Flaherty, N. T. Hahn, A. J. Bard and C. B. Mullins, *J. Phys. Chem. C*, 2011, **115**, 3794–3802.
2 A. Kudo, K. Ueda, H. Kato and I. Mikami, *Catal. Lett.*, 1998, **53**, 229–230.
3 C. Jiang, R. Wang and B. A. Parkinson, *ACS Comb. Sci.*, 2013, **15**, 639–645.
4 A. Walsh, Y. Yan, M. N. Huda, M. M. Al-Jassim and S.-H. Wei, *Chem. Mater.*, 2009, **21**, 547–551.
5 Y. Park, K. J. McDonald and K.-S. Choi, *Chem. Soc. Rev.*, 2013, **42**, 2321–2337.
6 S. Tokunaga, H. Kato and A. Kudo, *Chem. Mater.*, 2001, **13**, 4624–4628.
7 I. Vinke, J. Diepgrond, B. Boukamp, K. Vries and A. Burggaaf, *Solid State Ionics*, 1992, **57**, 83–89.
8 A. Kudo, K. Omori and H. Kato, *J. Am. Chem. Soc.*, 1999, **121**, 11459–11467.
9 Z.-F. Huang, L. Pan, J.-J. Zou, X. Zhang and L. Wang, *Nanoscale*, 2014, **6**, 14044–14063.
10 J. Yu and A. Kudo, *Adv. Funct. Mater.*, 2006, **16**, 2163–2169.
11 A. Iwase and A. Kudo, *J. Mater. Chem.*, 2010, **20**, 7536.
12 M. T. McDowell, M. F. Lichterman, J. M. Spurgeon, S. Hu, I. D. Sharp, B. S. Brunschwig and N. S. Lewis, *J. Phys. Chem. C*, 2014, **118**, 19618–19624.
13 K. Sayama, A. Nomura, T. Arai, T. Sugita, R. Abe, M. Yanagida, T. Oi, Y. Iwasaki, Y. Abe and H. Sugihara, *J. Phys. Chem. B*, 2006, **110**, 11352–11360.
14 K. Sayama, A. Nomura, Z. Zou, R. Abe, Y. Abe and H. Arakawa, *Chem. Commun.*, 2003, 2908.
15 P. Chatchai, Y. Murakami, S.-Y. Kishioka, A. Y. Nosaka and Y. Nosaka, *Electrochim. Acta*, 2009, **54**, 1147–1152.
16 T. H. Jeon, W. Choi and H. Park, *Phys. Chem. Chem. Phys.*, 2011, **13**, 21392–21401.
17 K. P. S. Parmar, H. J. Kang, A. Bist, P. Dua, J. S. Jang and J. S. Lee, *ChemSusChem*, 2012, **5**, 1926–1934.
18 H. S. Park, K. E. Kweon, H. Ye, E. Paek, G. S. Hwang and A. J. Bard, *J. Phys. Chem. C*, 2011, **115**, 17870–17879.
19 J. A. Seabold and K.-S. Choi, *J. Am. Chem. Soc.*, 2012, **134**, 2186–2192.
20 C. Ding, J. Shi, D. Wang, Z. Wang, N. Wang, G. Liu, F. Xiong and C. Li, *Phys. Chem. Chem. Phys.*, 2013, **15**, 4589–4595.
21 F. F. Abdi and R. van de Krol, *J. Phys. Chem. C*, 2012, **116**, 9398–9404.
22 J. A. Seabold, K. Zhu and N. R. Neale, *Phys. Chem. Chem. Phys.*, 2014, **16**, 1121–1131.
23 W. Luo, Z. Li, T. Yu and Z. Zou, *J. Phys. Chem. C*, 2012, **116**, 5076–5081.
24 S. K. Pilli, T. E. Furtak, L. D. Brown, T. G. Deutsch, J. A. Turner and A. M. Herring, *Energy Environ. Sci.*, 2011, **4**, 5028.
25 M. Zhou, J. Bao, Y. Xu, J. Zhang, J. Xie, M. Guan, C. Wang, L. Wen, Y. Lei and Y. Xie, *ACS Nano*, 2014, **8**, 7088–7098.
26 W. Luo, Z. Yang, Z. Li, J. Zhang, J. Liu, Z. Zhao, Z. Wang, S. Yan, T. Yu and Z. Zou, *Energy Environ. Sci.*, 2011, **4**, 4046–4051.
27 W. Yao, H. Iwai and J. Ye, *Dalton Trans.*, 2008, 1426–1430.
28 L. Chen, F. M. Toma, J. K. Cooper, A. Lyon, Y. Lin, I. D. Sharp and J. W. Ager, *ChemSusChem*, 2015, **8**, 1066–1071.
29 K. Ding, B. Chen, Z. Fang, Y. Zhang and Z. Chen, *Phys. Chem. Chem. Phys.*, 2014, **16**, 13465–13476.
30 H. Ye, J. Lee, J. S. Jang and A. J. Bard, *J. Phys. Chem. C*, 2010, **114**, 13322–13328.
31 D. K. Zhong, S. Choi and D. R. Gamelin, *J. Am. Chem. Soc.*, 2011, **133**, 18370–18377.
32 S. K. Cho, H. S. Park, H. C. Lee, K. M. Nam and A. J. Bard, *J. Phys. Chem. C*, 2013, **117**, 23048–23056.
33 H. Ye, H. S. Park and A. J. Bard, *J. Phys. Chem. C*, 2011, **115**, 12464–12470.
34 H. S. Park, H. C. Lee, K. C. Leonard, G. Liu and A. J. Bard, *ChemPhysChem*, 2013, **14**, 2277–2287.
35 M. de Respinis, K. S. Joya, H. J. M. De Groot, F. D'Souza, W. A. Smith, R. van de Krol and B. Dam, *J. Phys. Chem. C*, 2015, **119**, 7275–7281.
36 R. Li, H. Han, F. Zhang, D. Wang and C. Li, *Energy Environ. Sci.*, 2014, **7**, 1369–1376.
37 S. K. Choi, W. Choi and H. Park, *Phys. Chem. Chem. Phys.*, 2013, **15**, 6499–6507.
38 J. H. Kim, J. W. Jang, H. J. Kang, G. Magesh, J. Y. Kim, J. H. Kim, J. Lee and J. S. Lee, *J. Catal.*, 2014, **317**, 126–134.
39 F. Lin, D. Wang, Z. Jiang, Y. Ma, J. Li, R. Li and C. Li, *Energy Environ. Sci.*, 2012, **5**, 6400.
40 M. F. Lichterman, M. R. Shaner, S. G. Handler, B. S. Brunschwig, H. B. Gray, N. S. Lewis and J. M. Spurgeon, *J. Phys. Chem. Lett.*, 2013, **4**, 4188–4191.
41 Y. Liang and J. Messinger, *Phys. Chem. Chem. Phys.*, 2014, **16**, 12014–12020.
42 W. He, R. Wang, L. Zhang, J. Zhu, X. Xiang and F. Li, *J. Mater. Chem. A*, 2015, **3**, 17977–17982.
43 Y. H. Ng, A. Iwase, A. Kudo and R. Amal, *J. Phys. Chem. Lett.*, 2010, **1**, 2607–2612.
44 P. M. Rao, L. Cai, C. Liu, I. S. Cho, C. H. Lee, J. M. Weisse, P. Yang and X. Zheng, *Nano Lett.*, 2014, **14**, 1099–1105.
45 S. K. Pilli, R. Janarthanan, T. G. Deutsch, T. E. Furtak, L. D. Brown, J. A. Turner and A. M. Herring, *Phys. Chem. Chem. Phys.*, 2013, **15**, 14723–14728.

46 H. W. Jeong, T. H. Jeon, J. S. Jang, W. Choi and H. Park, *J. Phys. Chem. C*, 2013, **117**, 9104–9112.
47 P. Chatchai, S.-Y. Kishioka, Y. Murakami, A. Y. Nosaka and Y. Nosaka, *Electrochim. Acta*, 2010, **55**, 592–596.
48 Y. Liang, T. Tsubota, L. P. A. Mooij and R. van de Krol, *J. Phys. Chem. C*, 2011, **115**, 17594–17598.
49 R. Gutkowski and W. Schuhmann, *Phys. Chem. Chem. Phys.*, 2016, **18**, 10758–10763.
50 A. Kongkanand, R. M. Domínguez and P. V. Kamat, *Nano Lett.*, 2007, **7**, 676–680.
51 J. Resasco, H. Zhang, N. Kornienko, N. Becknell, H. Lee, J. Guo, A. L. Briseno and P. Yang, *ACS Cent. Sci.*, 2016, **2**, 80–88.
52 X. Chen, N. Li, K. Eckhard, L. Stoica, W. Xia, J. Assmann, M. Muhler and W. Schuhmann, *Electrochem. Commun.*, 2007, **9**, 1348–1354.
53 S. Schwamborn, M. Etienne and W. Schuhmann, *Electrochem. Commun.*, 2011, **13**, 759–762.
54 J. K. Cooper, S. Gul, F. M. Toma, L. Chen, Y.-S. Liu, J. Guo, J. W. Ager, J. Yano and I. D. Sharp, *J. Phys. Chem. C*, 2015, **119**, 2969–2974.
55 E. Kemppainen, A. Bodin, B. Sebok, T. Pedersen, B. Seger, B. Mei, D. Bae, P. C. K. Vesborg, J. Halme, O. Hansen, P. D. Lund and I. Chorkendorff, *Energy Environ. Sci.*, 2015, **8**, 2991–2999.
56 P. Salvador, *J. Phys. Chem.*, 1985, **89**, 3863–3869.
57 P. Salvador and C. Gutiérrez, *J. Electroanal. Chem.*, 1984, **160**, 117–130.
58 L. Peter, *Chem. Rev.*, 1990, **90**, 753–769.
59 C. Y. Cummings, F. Marken, L. Peter, A. A. Tahir and K. G. U. Wijayantha, *Chem. Commun.*, 2012, **48**, 2027–2029.
60 L. Peter, K. G. U. Wijayantha and A. A. Tahir, *Faraday Discuss.*, 2012, **155**, 309–322.
61 L. J. Brillson and Y. Lu, *J. Appl. Phys.*, 2011, **109**, 121301.
62 S. P. Berglund, A. J. E. Rettie, S. Hoang and C. B. Mullins, *Phys. Chem. Chem. Phys.*, 2012, 7065–7075.
63 S. M. Thalluri, C. Martinez Suarez, M. Hussain, S. Hernandez, A. Virga, G. Saracco and N. Russo, *Ind. Eng. Chem. Res.*, 2013, **52**, 17414–17418.
64 W.-J. Yin, S.-H. Wei, M. M. Al-Jassim, J. Turner and Y. Yan, *Phys. Rev. B: Condens. Matter Mater. Phys.*, 2011, **83**.
65 L. W. Shan, G. L. Wang, J. Suriyaprakash, D. Li, L. Z. Liu and L. M. Dong, *J. Alloys Compd.*, 2015, **636**, 131–137.
66 M. Wang, H. Zheng, J. Liu, D. Dong, Y. Che and C. Yang, *Mater. Sci. Semicond. Process.*, 2015, **30**, 307–313.